



# Recognition of multivariate geochemical anomalies associated with mineralization using an improved generative adversarial network

Chunjie Zhang, Renguang Zuo<sup>\*</sup>

*State Key Laboratory of Geological Processes and Mineral Resources, China University of Geosciences, Wuhan 430074, China*



## ARTICLE INFO

**Keywords:**

Generative adversarial network  
Adversarially learned anomaly detection  
Deep learning  
Geochemical anomalies  
Mineral exploration

## ABSTRACT

Deep learning (DL) algorithms have a strong ability to recognize high-level features in geochemical exploration data and have been widely employed for the recognition of multivariate geochemical anomalies linked to mineralization. In this study, the adversarially learned anomaly detection (ALAD) algorithm, an improved generative adversarial network (GAN), was employed to detect multivariate geochemical anomalies related to mineralization. Compared with other unsupervised deep learning algorithms, ALAD significantly improves anomaly detection performance by combining the advantages of deep variational autoencoder and generative adversarial network. Various experiments were performed to construct a well-designed network structure to process high-dimensional geochemical data to identify geochemical anomalies linked to tungsten (W) polymetallic mineralization in the south of Jiangxi Province of China. The extracted geochemical anomalies have a high spatial distribution correction with the locations of the discovered W polymetallic mineralization. Both the area under the receiver operating characteristic curve and the prediction-area plot indicate a good performance of the ALAD model. Furthermore, the extracted geochemical anomalies are spatially correlated with granites which control the spatial distribution of W polymetallic mineralization. These observations indicate that, as an unsupervised deep learning algorithm, ALAD is useful for detecting geochemical anomalies associated with mineralization.

## 1. Introduction

The identification of geochemical anomalies has played a significant role in mineral exploration over past few decades (e.g., Cheng, 1999; Carranza, 2009; Zuo et al., 2019). Geochemical anomalies can be defined as deviations from a normal background pattern (Rose et al., 1979). Recently, machine learning (ML) algorithms have been introduced for the identification of multivariate geochemical anomalies linked to mineralization (e.g., Chen and Wu, 2017; Sun et al., 2009; Wang et al., 2019; Xiong and Zuo, 2016, 2020). Compared to traditional approaches, such as probability graphs (Sinclair, 1974), multivariate statistics (Filzmoser et al., 2005), and fractal/multifractal models (Cheng et al., 1994, 2000), ML methods have exhibited huge potential in dealing with non-linear and high-dimensional geoscientific data due to its strong ability to extract automatically high-level representations from complex data (Reichstein et al., 2019). In geochemical exploration, ML methods have proven a powerful capacity to enhance the identification of geochemical anomalies and the recognition of hidden patterns (Zuo et al., 2019; Xiong and Zuo, 2020).

ML algorithms can be categorized as supervised and unsupervised learning methods. In supervised learning, the identification of geochemical anomalies is usually regarded as a process of classifying samples as being background or anomalous. The background is usually regarded as the negative sample and the anomaly usually is considered as the positive sample. Therefore, a binary classifier must be trained from an abundant dataset with positive and negative labels, such as convolutional neural networks (Li et al., 2020, 2021). Nevertheless, owing to the complexity of geological processes and the rarity of mineralization, labeled samples are often difficult to delineate and accurately tag. Besides, the imbalance between positive and negative samples also leads to its classifier failing to achieve good performance (Chawla et al., 2004; Zhou and Liu, 2006; Xiong and Zuo, 2018). Unsupervised algorithms are not dependent on the sample labels. Consequently, various unsupervised ML methods have been developed for identifying geochemical anomalies (e.g., Clare and Cohen, 2001; Chen and Wu, 2017; Xiong and Zuo, 2020).

The anomaly detection methods based on unsupervised algorithms are briefly summarized below. One of the main anomaly detection

\* Corresponding author.

E-mail address: [zrguang@cug.edu.cn](mailto:zrguang@cug.edu.cn) (R. Zuo).

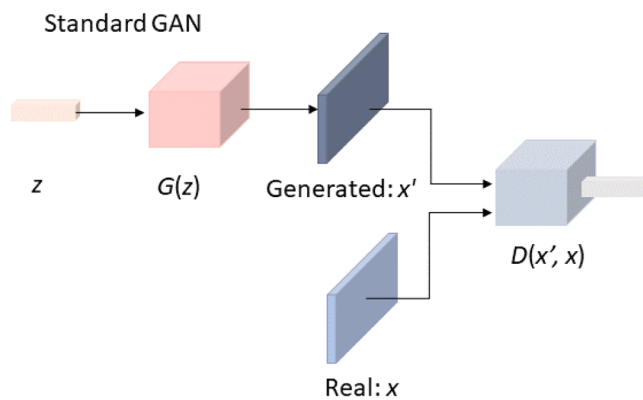


Fig. 1. A basic GAN framework.

methods is usually based on the distance, which assesses whether data are anomalous regarding their similarity from the nearest data neighbors or clusters at a specific distance (e.g., Chandola et al., 2009; Chen et al., 2020). For example, K-means, K-medoids, fuzzy c-means, and other traditional cluster methods divide geospatial data into homogeneous groups to detect geochemical anomalies (Vriend et al., 1988; Lacassie et al., 2006; Ghezelbash et al., 2020). Ghezelbash et al. (2020) used a genetic K-means clustering algorithm for optimal anomaly detection. Chen et al. (2020), Chen et al. (2021) identified geochemical anomalies associated with Au deposits based on distance anomaly factors. Such an approach relies on distance metric which is suitable for the data (Zenati et al., 2018b). Another class of anomaly detection method is to determine the boundary of the normal data. For example, the one-class support vector machine (SVM) (Olkopf et al., 2000) has been adopted to identify geochemical anomalies (Chen and Wu, 2017). The third method is based on the reconstruction error to identify the anomaly like autoencoder networks (e.g., Xiong and Zuo, 2016, 2021; Luo et al., 2020). The principle of autoencoder networks is that normal samples can be well reconstructed and have low reconstruction errors. Abnormal samples cannot be well reconstructed and have high reconstruction errors.

Recently, further studies have focused on deep learning algorithms, such as deep autoencoders and variational autoencoders (Xiong and Zuo, 2016, 2020; Chen et al., 2019; Luo et al., 2020) that were successfully employed to identify multivariate geochemical anomalies

owing to their ability to extract features automatically. Deep autoencoders first train a model to learn pattern distribution of the samples to reconstruct samples and subsequently determine samples with high reconstruction errors as anomalies. The generative adversarial network (GAN) (Goodfellow et al., 2014) has been widely applied to various fields because of its strong ability to learn highly structured probability distributions (Goodfellow et al., 2014; Larsen et al., 2016; Schlegl et al., 2017; Li et al., 2017a; Li et al., 2017b; Radford et al., 2015; Salimans et al., 2016; Theis et al., 2015). Compared to deep variational autoencoder (VAE) techniques (Kingma and Welling, 2013), GAN-based approaches can produce high-quality samples without immolating sampling speed and take advantage of the latent representation in the process of generation (Dumoulin et al., 2017). Besides, compared with the conventional autoencoder framework, the GAN framework adds a discriminator that has a role in regulating feedback and guiding the generator. Therefore, GAN has become a powerful generation network for learning discretionary complex data distribution and modeling complex high-dimensional datasets (Goodfellow et al., 2014; Donahue et al., 2017).

Schlegl et al. (2017) proposed AnoGAN to identify anomaly detection in the field of medical images; Zenati et al. (2018a) proposed an efficient GAN architecture for anomaly detection. Concurrently, GANomaly (Akcay et al., 2018) was proposed for anomaly detection. Although GAN and its variants have been introduced into the domain of anomaly detection (e.g., Schlegl et al., 2017; Zenati et al., 2018a), GAN models also have shortcomings, being difficult to train and unstable (Goodfellow et al., 2014). Compared with VAE, GAN lacks an effective inference mechanism, which hinders them from performing abstract reasoning on data. Therefore, some works are devoted to breaking the gap between VAE and GAN to learn an inference mechanism while building a high-quality generative model (Dumoulin et al., 2017; Larsen et al., 2016).

The adversarially learned anomaly detection (ALAD) (Zenati et al., 2018b), which combines the advantages of VAE and GAN, imbeds an inference network (or encoder) and a deep generative network (or decoder) into an adversarial framework. Furthermore, additional discriminators were used for improving the ability of the encoder and generator, and the spectral normalization method (Miyato et al., 2018) was adopted to stabilize the GAN because of its difficulty in training. In contrast to other GAN models, ALAD learns from the latent variables to generate sample data and learns the inverse mapping from data to latent

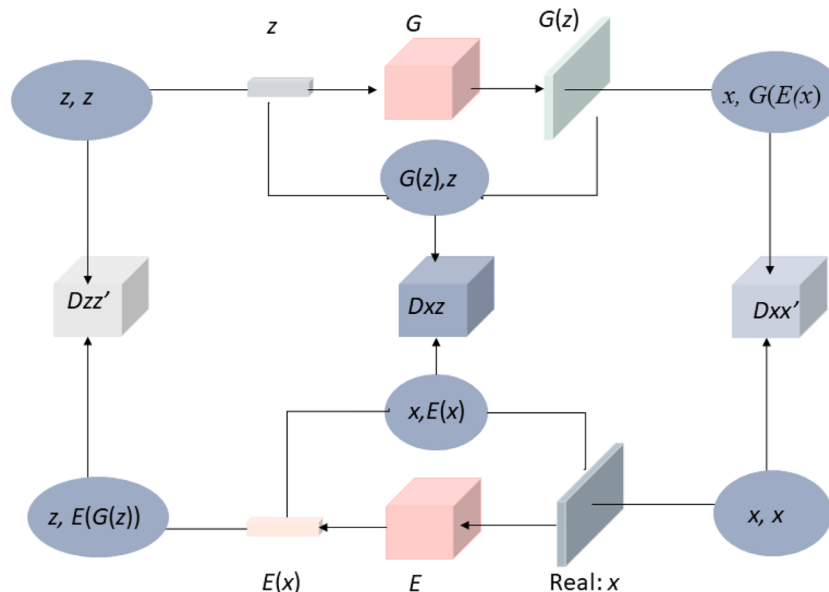
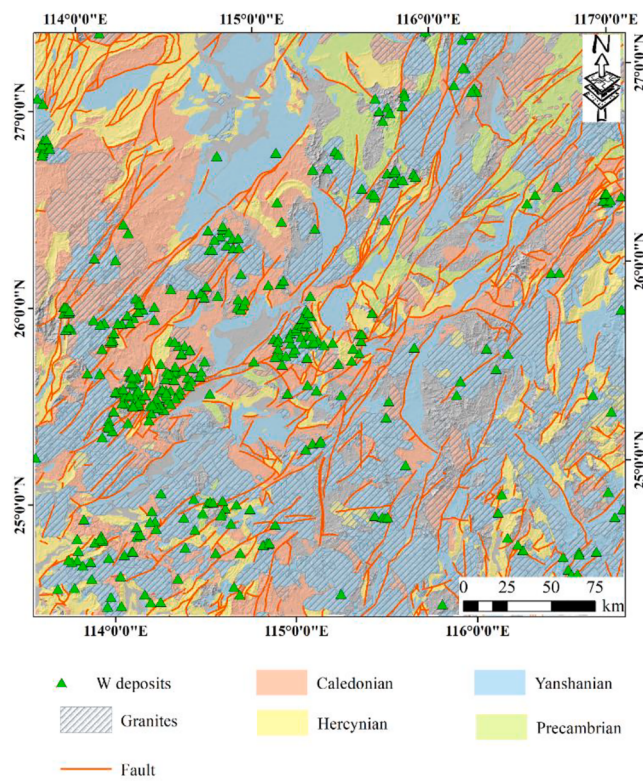


Fig. 2. An adversarial learning anomaly detection method.



**Fig. 3.** A simplified geological map of the south Jiangxi province of China.

representation. ALAD belongs to the reconstruction-based anomaly detection method by evaluating the difference between the real sample and its reconstruction. In contrast to the deep autoencoder network, the improvement of ALAD is that the anomaly scores can infer not only whether the sample can be reconstructed well, but also whether the sample derived from the real data distributions can be well encoded. Therefore, ALAD has a strong capacity to capture anomalies.

In this study, the ALAD model was employed to process high-dimensional geochemical data to extract multivariate geochemical anomalies related to tungsten (W) polymetallic mineralization in the south of Jiangxi Province, China, for guiding further mineral exploration in this region.

## 2. Methods

### 2.1. Generative adversarial network

The basic generative adversarial network (GAN) model places the generation mode  $G$  and the discriminant model  $D$  into an adversarial

**Table 1**  
Network parameters in ALAD model.

	Operation	Units	Non linearity	Dropout
$E(x)$	Dense	256	LReLU	0
	Dense	128	LReLU	0
	Dense	64	None	0
$G(z)$	Dense	128	LReLU	0
	Dense	256	LReLU	0
	Dense	274	None	0
$D_{xz}$	only $x$			
	Dense	128	LReLU	0
	only $z$			
	Dense	128	LReLU	0.5
	Concatenate outputs			
	Dense	256	LReLU	0.5
$D_{xx'}$	Dense	1	Sigmoid	0
	Concatenate $x$ and $x'$			
	Dense	256	LReLU	0.2
	Dense	128	LReLU	0.2
	Dense	1	Sigmoid	0
	Concatenate $z$ and $z'$			
$D_{zz'}$	Dense	64	LReLU	0.2
	Dense	32	LReLU	0.2
	Dense	1	Sigmoid	0
	Optimizer			
Batch Size	Adam			
Epochs	128			
Learning rate	100			
	0.0001			

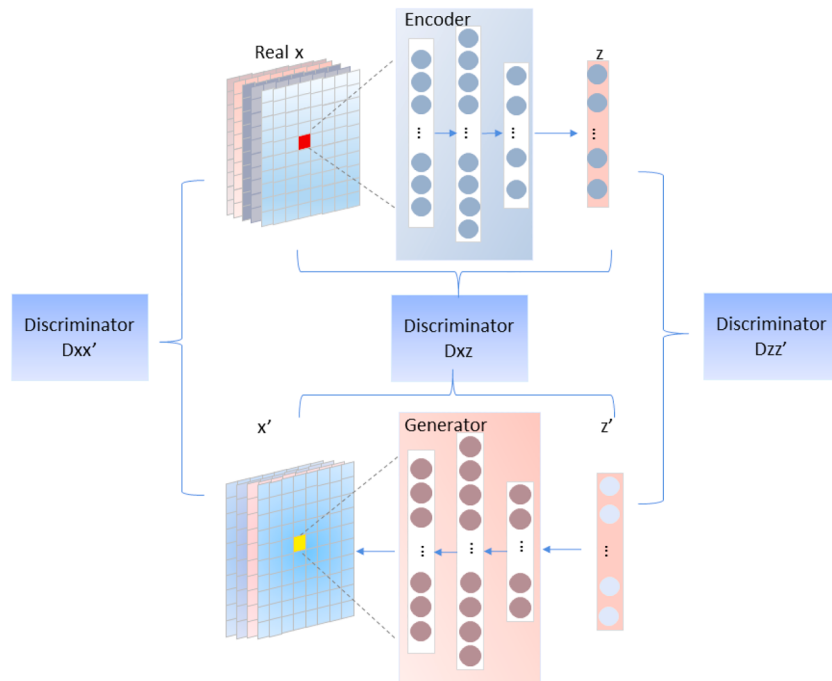


**Fig. 4.** A designed ALAD model.

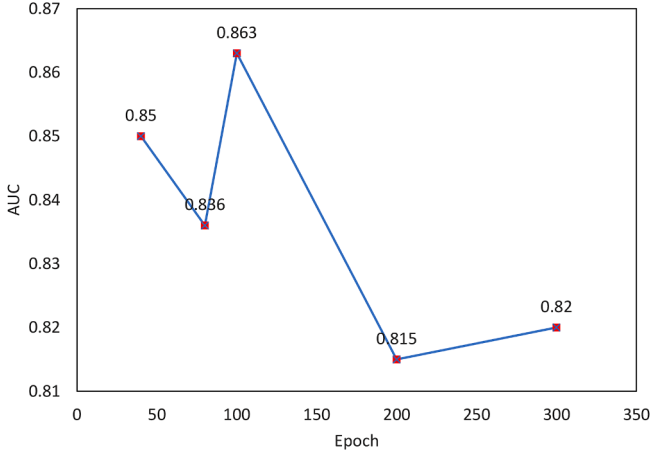


Fig. 5. AUCs with different epochs.

process. The generative model  $G$  is used to learn the data distribution, and a discriminative model  $D$  is used to assess the probability of a sample coming from real data, not  $G$  (Goodfellow et al., 2014) (Fig. 1). In GAN framework, the input noise variables  $p_z(z)$  must be given and mapped in data space as  $G(z)$  through the  $G$  model through learning the generator's distribution  $p_g$  over data  $x$ .  $D(x)$  outputs a single scalar that denotes the probability that  $x$  is derived from the data rather than  $G(z)$ . Therefore, training  $D$  aims to maximize the probability to distinguish between real samples and samples from  $G$ . Synchronously,  $G$  is trained to generate samples to fool the discriminative model  $D$  by minimizing  $\log(1-D(G(z)))$ . Differently expressed,  $D$  and  $G$  conduct a two-player minimax confrontation game with a function  $V(G, D)$  value as follows:

$$\min_{G} \max_{D} V(D, G) = E_{x \sim p_{\text{data}}(x)}[\log D(x)] + E_{z \sim p_z(z)}[\log(1 - D(G(z)))] \quad (1)$$

## 2.2. An improved GAN architecture

Considering that the original GAN is used mainly for model generation rather than anomaly detection, the ALAD algorithm optimizes and improves the basic GAN model. In the basic GAN framework (Goodfellow et al., 2014), only the generator mapped latent samples to generate data but did not contain the process of inversely mapping data to the latent representation. Therefore, the ALAD model builds a framework that can concurrently learn an encoder network  $E$  that maps data sample  $x$  to the latent space  $z$  and learn the generator  $G$  that maps latent  $z$  into generator data  $G(z)$  (Dumoulin et al., 2017; Donahue et al., 2017). In such a model, the approximate representation of data point  $x$  can be calculated briefly by passing  $x$  through the encoder  $E$ . A discriminator  $D_{xz}$  was used to evaluate the probability that a sample was derived from real data instead of the generator  $G$ . Also, the model incorporated recent improvements to improve the encoder network (Li et al., 2017a, 2017b) by adding two additional discriminator  $D_{zz'}$  and  $D_{xx'}$  to encourage cycle consistency (Zenati et al., 2018b), i.e., making  $E(G(z))$  close to  $z$ . An ALAD framework (Fig. 2) includes an encoder, a generator, and three discriminators  $D_{xz}$ ,  $D_{xz'}$ , and  $D_{zz'}$ .

**Encoder:** The model adds an encoder  $E$  for mapping data  $x$  to latent representations  $z$ , which aims to capture the approximate representation of real data point  $x$  through encoding quickly.

**Generator:** Similar to the traditional GAN, the input noise variables  $z$  must be defined. Through the generator, the  $z$  is mapped in data space  $G(z)$ .

**$D_{xz}$ :** The discriminator  $D_{xz}$  not only discriminates  $x$  and  $E(x)$  in data space but also needs to distinguish  $G(z)$  and  $z$  in latent space. The jointly tuples  $((x; E(x))$  versus  $(G(z); z)$ ) are used as the input to fool  $D_{xz}$  (Fig. 2). The generator  $G$  and the encoder  $E$  are trained to minimize  $G$ ,  $E$  and maximize  $D_{xz}$  with  $V(D_{xz}, E, G)$ , which is defined as:

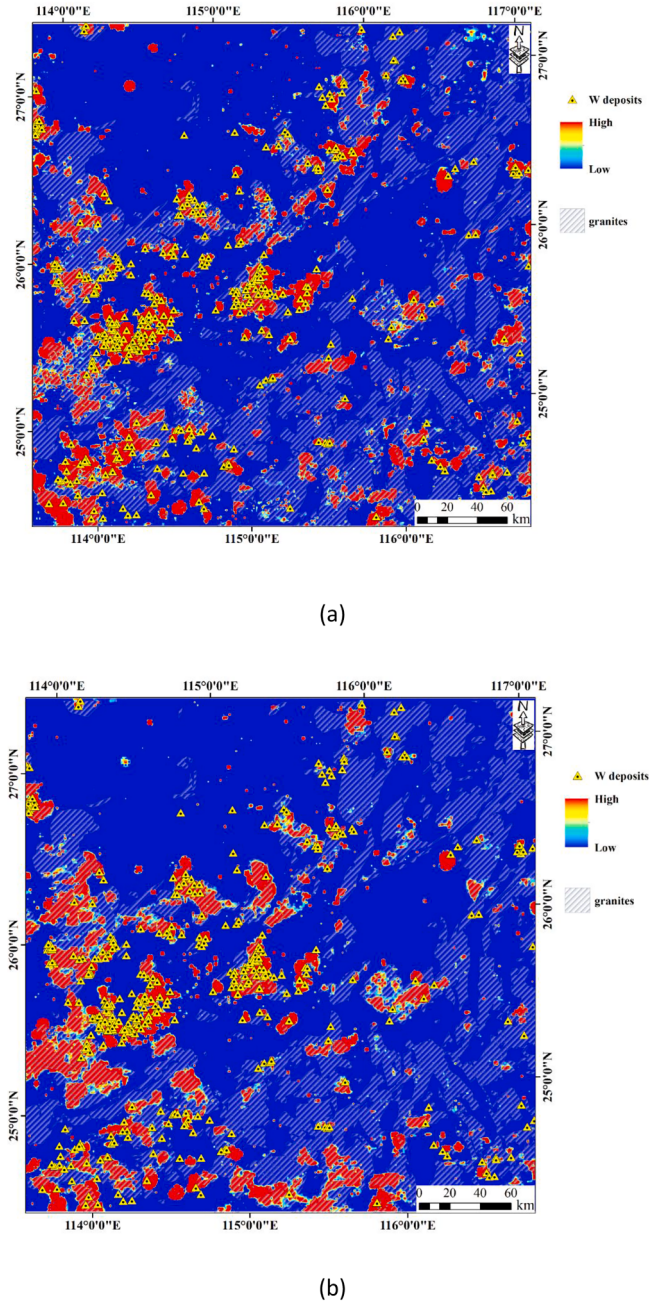


Fig. 6. Map showing the detected geochemical anomalies obtained by (a) ALAD and (b) VAE, respectively.

$$V(D_{xz}, E, G) = E_{x \sim p_x}[ \log D_{xz}(x, E(x)) ] + E_{z \sim p_z}[ 1 - \log D_{xz}(G(z), z) ] \quad (2)$$

**$D_{xx'}$ :** An additional discriminator network  $D_{xx'}$  is used to force cycle consistency (Li et al., 2017a, 2017b). The discriminator network  $D_{xx'}$  aims to make  $G(E(x))$  close to  $x$ .  $G(E(x))$  represents a reconstruction value that is first encoded by the encoder  $E(x)$ , and then reconstructed by the generator  $G$ . The jointly tuples  $((x; x)$  versus  $(x, G(E(x)))$  are used as the input to train the  $D_{xx'}$ . It can be defined as:

$$V(D_{xx'}, E, G) = E_{x \sim p_x}[ \log D_{xx'}(x, x) ] + E_{x \sim p_x}[ 1 - \log D_{xx'}(x, G(E(x))) ] \quad (3)$$

**$D_{zz'}$ :** An additional adversarially learned discriminator  $D_{zz'}$ , which aims to make  $E(G(z))$  close to  $z$ , is used to regularize the latent space conditional.  $E(G(z))$  means the underlying representation in latent space that  $G(z)$  is first generated by inputting the random latent variable  $z$  through the generator  $G$ , and then encoded by the  $E$ . The jointly tuples

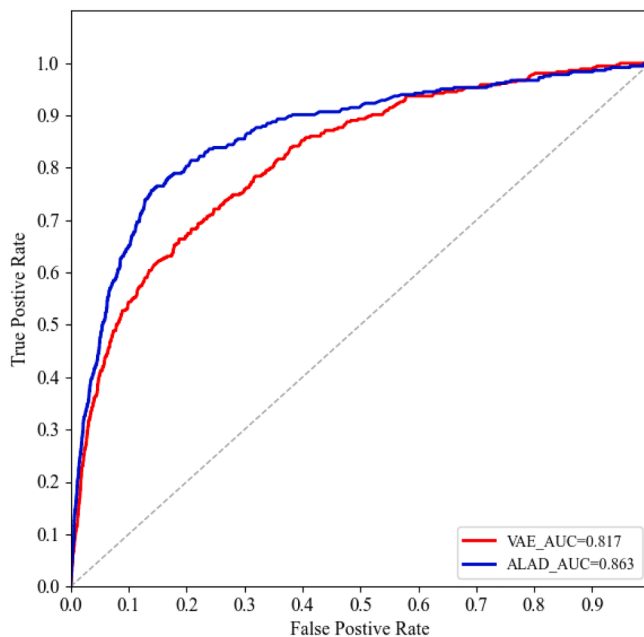


**Fig. 7.** ROC plots for geochemical anomalies obtained by ALAD and VAE.

$((z; z)$  versus  $(z, E(G(z)))$ ) are used as the input to fool the  $D_{zz'}$ . It is defined as:

$$V(D_{zz'}, E, G) = E_{\tilde{p}Z}[\log D_{zz'}(z, z)] + E_{\tilde{p}Z}[1 - \log D_{zz'}(z, E(G(z)))] \quad (4)$$

Recent studies (Gulrajani et al., 2017; Miyato et al., 2018) demonstrated the potency by adding Lipschitz constraints to GAN discriminators to maintain the training stability. In this model, the conditional distribution is further regularized by attaching another conditional entropy constraint and spectral normalization (Miyato et al., 2018) was employed to regularize the encoder (Zenati et al., 2018b). The model aims to minimize  $G, E$  and maximize  $D_{xz}, D_{xx'}, D_{zz'}$  during training with a defined value  $V(D_{xz}, D_{xx'}, D_{zz'}, E, G)$  as follows:

$$V(D_{xz}, D_{xx'}, D_{zz'}, E, G) = V(D_{xz}, E, G) + V(D_{xx'}, E, G) + V(D_{zz'}, E, G) \quad (5)$$

### 2.3. Detecting anomalies

ALAD evaluates the difference between samples and their reconstructions based on the GAN. Normal samples can be well-reconstructed, while anomalous samples are likely not to be well-reconstructed (Zenati et al., 2018b). The model learns the multiformality pattern of the data to restore an accurate underlying representation to reconstruct the normal sample faithfully. The anomaly score is calculated by quantifying the difference between the real samples and their reconstruction. In this model, the distance between samples  $x$  and  $G(E(x))$  is chosen as the final anomaly scores. A score function  $A(x)$  was calculated based on the  $L_1$  reconstruction error followed as:

$$A(x) = \|f_{xx}(x, x) - f_{xx}(x, G(E(x)))\|_1 \quad (6)$$

Here,  $f(\cdot, \cdot)$  represents the activation function in  $D_{xx'}$  network.  $A(x)$  can measure the confidence of the discriminator that a sample is well encoded by the trained encoder  $D$  and reconstructed by trained generator  $G$  deriving from the real data distribution. The samples with higher values of  $A(x)$  represent poorly reconstructed and are more likely to be regarded as anomalies.

## 3. Study area and dataset

### 3.1. Geological setting

The study area is located in the south of Jiangxi Province of China (Fig. 3). Previous works have shown that world-class tungsten deposits exist in this district, such as Dajishan, Yaogang, and Xihuashan deposits (Peng et al., 2006; Liu et al., 2014). The South China geological structure is composed of the Northwest Yangtze Craton and the Southeast Cathaysia Block, formed in a subduction collision event of approximately ca. 970 Ma (Li and McCulloch, 1996). The Jiangnan orogenic belt is formed between the Yangtze Craton and the Cathaysia Block. It is about 1500 km long and consists of Precambrian metamorphic sedimentary sequences and igneous rocks (Zhao and Cawood, 1999; Huang and Jiang, 2014; Wang and Shu, 2012; Wang et al., 2015; Zhao, 2015). The basement of the orogenic belt consists of two sets of metasedimentary strata (Zhao, 2015; Zhao et al., 2017; Zhou et al., 2009). In Neoproterozoic, some sedimentary rocks were transformed into metamorphic rock (Wang and Zi, 2007; Gao et al., 2008, 2012). The faults, intrusive rocks, and mineralization were mainly affected by Neoproterozoic tectonic and Mesozoic tectonic activity, which brought forth ductile shear zones, nappe structures, folds of different scales, and rift

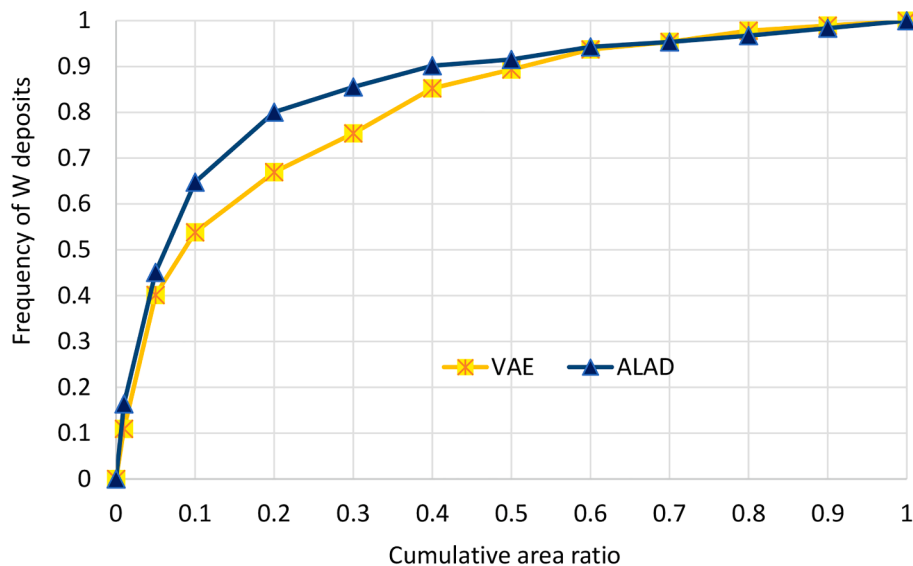


**Fig. 8.** Prediction-area (P-A) plots for geochemical anomalies of ALAD and VAE.

basins (Xu et al., 1992; Yang et al., 2009; Wang et al., 2017; Gao et al., 2008). The Mesozoic lithosphere stretched to form granitic and volcanic rocks, resulting in large-scale mineralization (Zhou et al., 2006; Wang and Shu, 2012). The frequent structural and geological activities produced various faults and folds, which provided favorable spaces and channels for the migration of ore-forming hydrothermal fluids (Fang et al., 1999; Wang et al., 2017).

### 3.2. Geochemical data

The data used in this study is compiled from the National Geochemical Surveying and Mapping Project of China (Wang et al., 2007; Xie et al., 1997). Standardized stream sediment sampling was collected from mountainous and hilly regions of China with an average sampling density of approximately 1 sample/km<sup>2</sup>. Composite samples from 4 km<sup>2</sup> were submitted to the laboratories to reduce the number of samples for multi-element analysis. The 32 elements including Ag, As, Au, B, Ba, Be, Bi, Cd, Co, Cr, Cu, F, Hg, La, Li, Mn, Mo, Nb, Ni, P, Pb, Sb, Sn, Sr, Th, Ti, U, V, W, Y, Zn, and Zr, and 7 major elements Al, Fe, Ca, Mg, K, Na, and Si were determined (Xie and Ren, 1993). A single moving average method with a 4 × 4 km or 6 × 6 km moving window and a 2 km moving step was used to preprocess the original data for evenly mixing the collected samples data to represent this area (Xie et al., 1997). Therefore, according to the previous studies (e.g., Chi et al., 2012; Gong et al., 2015; Liu et al., 2013; Wu et al., 2006), five geochemical elements (Ag-Bi-Mo-Sn-W) related to W polymetallic mineralization were selected as pathfinders to ascertain geochemical anomalies related to W-polymetallic mineralization.

## 4. Result and discussion

### 4.1. Experimental setup

In the experiment, the related geochemical data were interpolated into grid data with a cell size of 500 m × 500 m using the inverse distance weighted interpolation (Shepard, 1968). A total of 70% of the samples were adopted as the training set and the remaining were adopted as the testing set. All the programs were implemented based on the Python and Tensorflow libraries.

In the experiment, the encoder ( $E$ ) and the generator ( $G$ ) were designed (Fig. 4). A discriminator was used for guiding the generator ( $G$ ) and encoder ( $E$ ), and the additional discriminators were added to encourage cycle-consistency. Before training the network, several basic network settings were established to optimize the network. The Adam optimizer (Duchi et al., 2011) was applied in this model to estimate the first and second moments of the gradient and dynamically adjust the parameters of the learning rate. Simultaneously, the exponentially weighted moving average and offset correction were used to stabilize the parameter variation. The leaky Rectified Linear Units (ReLU) is a linear function that uses a predefined constant range from 0 to 1 to compress the negative input. In comparison to the ReLU activation function, the leaky ReLU function can retain negative information. Thus, except for the last layer of an encoder (no activation) and discriminator (using sigmoid activation), the encoder, decoder, and discriminator layers used leaky ReLU as the activation function.

To train the ALAD model optimally, some parameters such as the learning rates, the batch size, and the number of epochs, should be adjusted. Table 1 lists the parameters used in this study. The batch size and the learning rate were determined as 128 and 0.0001 via the trial and error. The iteration times can affect the result of detecting anomalies by ALAD. With too few epochs, the model will poorly learn the distribution pattern of the complex geochemical data, leading to a sub-optimal performance in constructing high-dimensional geochemical data. With too many epochs, the model tends to overfit, resulting in poor generalization ability. We set the epoch numbers to 40, 80, 100, and 200. The receiver operating characteristic (ROC) curve (Hanley and

Mcneil, 1983) and the area under the ROC curve (AUC) were adopted to evaluate the performance (e.g., Chen and Wu, 2017; Zuo, 2018). The AUC value closer to 1 suggests a better performance of the obtained results. The model achieved the best performance when the epoch number was set to 100 (Fig. 5).

### 4.2. Geochemical anomalies recognition

The anomaly probability map recognized by ALAD (Fig. 6a) shows that most known W polymetallic deposits are located in the regions with high anomaly scores, indicating that the detected geochemical anomalies have a strong spatial correlation with locations of the discovered mineral deposits. The other areas with high probability anomaly scores indicate the potential for the discovery of W polymetallic mineralization in this district. The geochemical anomaly map was compared with the anomalous map extracted by VAE (Fig. 6b). The spatial distribution of high anomalous areas obtained by the VAE is similar to the results of ALAD, indicating that both VAE and ALAD are useful for detecting multivariate geochemical anomalies associated with mineralization.

The AUC values of ALAD and VAE are 0.863 and 0.817 (Fig. 7), respectively, which means that the performance of ALAD is better than VAE. Furthermore, the prediction-area (P-A) plot was applied in evaluating the identified geochemical anomalies (Zuo et al., 2009; Yousefi and Carranza, 2015, 2016). The P-A curve of ALAD is distributed above the VAE (Fig. 8), meaning that the performance of ALAD is better than VAE. Meanwhile, the detected geochemical anomalies obtained by ALAD accounted for 5.0% of the whole study area and contained 80.0% of the total number of discovered mineral deposits (Fig. 8). These observations suggest that ALAD is an effective approach to detect multivariate geochemical anomalies linked to mineral deposits.

From a geological perspective, the detecting geochemical anomalies by ALAD are located in or near granites (Fig. 6a). Mesozoic granites are diffusely distributed in this region. Alkali feldspar granites and syenogranites are the principal mineralization rocks (Liu et al., 2014). Nanling Mesozoic ore-forming granite has experienced multiple stages of differentiation, evolution, emplacement, and mineralization, and has formed a characteristic of W-rich polymetallic elements (Mao and Tan, 1998; Liu et al., 2010, 2014). The formation of W-polymetallic deposits is mainly controlled by these granites (Liu et al., 2014). The anomalies detected by ALAD are consistent with the conclusion that granite is the principal mineralization rocks for W polymetallic mineralization, indicating that the results obtained by ALAD are credible. Detected geochemical anomalies can also provide a significant indicator for further mineral exploration in this region.

## 5. Conclusions

In this study, a GAN-based anomaly detection method was applied to detect multivariate geochemical anomalies related to W-polymetallic mineralization in the south Jiangxi Province, China. The anomaly probability map recognized by ALAD shows that most of the discovered W-polymetallic deposits are situated at areas linked to high anomaly scores, indicating a strong spatial correlation between the detected geochemical anomalies and the locations of W polymetallic mineralization. The other high probability anomalous areas but without known W polymetallic mineralization indicate the underlying possibility to discover new W polymetallic deposits in this region. In addition, AUC and P-A plots suggest the ALAD model has a superior performance, indicating its availability for detecting multivariate geochemical anomalies related to mineralization.

### Declaration of Competing Interest

The authors declare that they have no known competing financial interests or personal relationships that could have appeared to influence the work reported in this paper.

## Acknowledgements

We thank Prof. Xueqie Wang for providing geochemical data, Dr. Behnam Sadeghi, associate editor for Ore Geology Reviews, for handing our manuscript, and two anonymous reviewers' comments and suggestions which helped us improve this study. The research was supported by the National Natural Science Foundation of China (No. 41972303), and MOST Special Fund from the State Key Laboratory of Geological Processes and Mineral Resources, China University of Geosciences (MSFGPMR03-3).

## References

- Akcay, S., Atapour-Abarghouei, A., Breckon, T.P., 2018. GANomaly: Semi-supervised anomaly detection via adversarial training. *Asian Conf. Computer Vision* 622–637.
- Caranza, E.J.M., 2009. Geochemical anomaly and mineral prospectivity mapping in GIS. *Handbook of Exploration & Environmental Geochemistry* 11.
- Chandola, V., Banerjee, A., Kumar, V., 2009. Anomaly detection: A survey. *ACM Comput. Surv.* 41, 3.
- Chawla, N.V., Japkowicz, N., Kotz, A., 2004. Editorial: special issue on learning from imbalanced data sets. *ACM Sigkdd Explorations Newsletter* 6, 1–6.
- Chen, L., Guan, Q., Xiong, Y., Liang, J., Wang, Y., Xu, Y., 2019. A Spatially Constrained Multi-Autoencoder approach for multivariate geochemical anomaly recognition. *Comput. Geosci.* 125, 43–54.
- Chen, Y., Wu, W., 2017. Application of one-class support vector machine to quickly identify multivariate anomalies from geochemical exploration data. *Geochemistry: Exploration Environment. Analysis* 17, 231–238.
- Chen, Y., Sun, G., Zhao, Q., 2020. Detection of multivariate geochemical anomalies associated with gold deposits by using distance anomaly factors. *Journal of Geochemical Exploration* 221, 106704.
- Chen, Y., Sun, G., Zhao, Q., 2021. Distance anomaly factors for gold potential mapping in the Jinchanggouliang area, Inner Mongolia, China. *Earth Science Informatics*. <https://doi.org/10.1007/s12145-021-00614-5>.
- Cheng, Q., Agterberg, F.P., Ballantyne, S.B., 1994. The separation of geochemical anomalies from background by fractal methods. *J. Geochem. Explor.* 51, 109–130.
- Cheng, Q., 1999. Spatial and scaling modeling for geochemical anomaly separation. *J. Geochem. Explor.* 65, 175–194.
- Cheng, Q., Xu, Y., Grunsky, E., 2000. Integrated spatial and spectrum method for geochemical anomaly separation. *Nat. Resour. Res.* 9, 43–52.
- Chi, Q., Wang, X., Xu, S., Zhou, J., Liu, H., Liu, D., Zhang, B., Wang, W., 2012. Geochemical Spatial and Temporal Distribution of Tungsten and Tin in the South China Block. *Earth Science Fronties* 19 (3), 70–83.
- Clare, A.P., Cohen, D.R., 2001. A comparison of unsupervised neural networks and k-means clustering in the analysis of multi-element stream sediment data. *Geochemistry: Exploration Environment. Analysis* 1 (2), 119–134.
- Donahue, J., Krähénbühl, P., Darrell, T., 2017. Adversarial feature learning. *arXiv*: 1605.09782.
- Duchi, J., Hazan, E., Singer, Y., 2011. Adaptive subgradient methods for online learning and stochastic optimization. *J. Mach. Learn. Res.* 12, 2121–2159.
- Dumoulin, V., Belghazi, I., Poole, B., Mastropietro, O., Lamb, A., Arjovsky, M., 2017. Adversarially learned inference. *Int. Conf. Learn. Representations* [arXiv:1606.00704](https://arxiv.org/abs/1606.00704).
- Fang, W., Liu, J., Zhang, G., 1999. On metallogenic system of continental dynamics and characteristics of metallogenic series and prospecting orientation in the south Qinling and its vicinity areas. *Northwest Geosciences* 20 (2), 1–16.
- Filzmoser, P., Garrett, R.G., Reimann, C., 2005. Multivariate outlier detection in exploration geochemistry. *Comput. Geosci.* 31, 579–587.
- Gao, L., Huang, Z., Ding, X., Liu, Y., Pang, J., 2012. Zircon SHRIMP U-Pb dating of Xuishui and Majianqiao Formations in northwestern Jiangxi Province. *Geol. Bullet. China* 31, 1086–1093 (in Chinese with English abstract).
- Gao, L., Yang, M., Ding, X., Liu, Y., Liu, X., Ling, L., 2008. SHRIMP U-Pb zircon dating of tuff in the Shuangqiaoshan and Heshangshan groups in South China constraints on the evolution of the Jiangnan Neoproterozoic orogenic belt. *Geol. Bullet. China* 27 (10), 1744–1751 (in Chinese with English abstract).
- Ghezelbash, R., Maghsoudi, A., Carranza, E.J.M., 2020. Optimization of geochemical anomaly detection using a novel genetic K-means clustering (GKMC) algorithm. *Comput. Geosci.* 134, 104335.
- Gong, J., Li, F., Zhang, S., Cui, F., 2015. Delineating anomalies using similarity coefficients based on element assemblage characteristics: An example of the Nanling area. *Geol. Explorat.* 2, 312–322 (In Chinese with English abstract).
- Goodfellow, J., Pouget-Abadie, M., Mirza, B., Xu, D., Warde-Farley, S., Ozair, A., Courville, B., 2014. Generative adversarial nets. *Adv. Neural Inform. Process. Syst.* 27, 267–2680.
- Gulrajani, I., Ahmed, F., Arjovsky, M., Dumoulin, V., Courville, A.C., 2017. Improved training of wasserstein GAN. *Adv. Neural Inform. Process. Syst.* 30, 5767–5777.
- Hanley, J.A., Mcneil, B.J., 1983. A method of comparing the areas under receiver operating characteristic curves derived from the same cases. *Radiology* 148, 839–843.
- Huang, L., Jiang, S., 2014. Highly fractionated S-type granites from the gian Dahutang tungsten deposit in Jiangnan Orogen, Southeast China: geochronology, petrogenesis and their relationship with W-mineralization. *Lithos* 202, 207–226.
- Lacassie, J.P., Del Solar, J.R., Roser, B., Herve, F., 2006. Visualization of volcanic rock geochemical data and classification with artificial neural networks. *Math. Geol.* 38, 697–710.
- Larsen, A.B.L., Sønderby, S.K., Larochelle, H., Winther, O., 2016. Autoencoding beyond pixels using a learned similarity metric. *Int. Conf. Mach. Learn.* 48, 1558–1566.
- Li, C., Liu, H., Chen, C., Pu, Y., Chen, L., Henao, R., Carin L., 2017a. Alice: towards understanding adversarial learning for joint distribution matching. In: *Proceedings of the 31st International Conference on Neural Information Processing System* 17, 5501–5509.
- Li, H., Li, X., Yuan, F., Jowitt, S.M., Zhang, M., Zhou, J., Wu, B., 2020. Convolutional neural network and transfer learning based mineral prospectivity modeling for geochemical exploration of Au mineralization within the Guadian-Zhangbaling area, Anhui Province, China. *Appl. Geochem.* 122, 104747.
- Li, J., Monroe, W., Shi, T., Jean, S., Ritter, A., Jurafsky, D., 2017b. Adversarial learning for neural dialogue generation. *arXiv:1701.06547*.
- Li, T., Zuo, R., Xiong, Y., Peng, Y., 2021. Random-drop data augmentation of deep convolutional neural network for mineral prospectivity mapping. *Nat. Resour. Res.* 30, 27–38.
- Li, X., McCulloch, M.T., 1996. Secular variation in the Nd isotopic composition of Neoproterozoic sediments from the southern margin of the Yangtze Block: evidence for a Proterozoic continental collision in southeast China. *Precambrian Res.* 76, 67–76.
- Liu, S., Chen, Y., Fan, S., Xu, J., Qu, W., Ying, L., 2010. The Second Ore-Prospecting Space in the Eastern and Central Parts of the Nanling Metallogenic Belt: Evidence from Isotopic Chronology. *Geol. China* 37, 1034–1049 (in Chinese with English Abstract).
- Liu, Y., Cheng, Q., Xia, Q., Wang, X., 2013. Application of singularity analysis for mineral potential identification using geochemical data—A case study: Nanling W-Sn-Mo polymetallic deposit, South China. *J. Geochem. Explor.* 134, 61–72.
- Liu, Y., Cheng, Q., Xia, Q., Wang, X., 2014. Mineral potential mapping for tungsten polymetallic deposits in the Nanling metallogenic belt, South China. *J. Earth Sci.* 25, 789–790.
- Luo, Z., Xiong, Y., Zuo, R., 2020. Recognition of geochemical anomalies using a deep variational autoencoder network. *Appl. Geochem.* 122, 104710.
- Kingma, D. P., Welling, M., 2013. Auto-encoding variational bayes. *arXiv:1312.6114*.
- Mao, J., Tan, H., 1998. The geological and geochemical characteristics of Shizhuyuan W-Sn-Mo-Bi polymetallic deposit in southern Hunan province. *Geological Publishing House, Beijing* 34–56 (in Chinese with English abstract).
- Miyato, T., Kataoka, T., Koyama, M., Yoshida, Y., 2018. Spectral normalization for generative adversarial networks. *arXiv:1802.05957*.
- Olkopf, B.S., Williamson, R., Smola, A., Shawe-Taylor, J., Platt, J., 2000. Support vector method for novelty detection. *Adv. Neural Inform. Process. Syst.* 12, 582–588.
- Peng, J., Zhou, M., Hu, R., Shen, N., Yuan, S., 2006. Precise molybdenite Re-Os and mica Ar–Ar dating of the Mesozoic Yaogangxian tungsten deposit, central Nanling district, South China. *Miner. Deposita* 41, 661–669.
- Radford, A., Metz, L., Chintala, S., 2015. Unsupervised representation learning with deep convolutional generative adversarial networks. *arXiv:1511.06434*.
- Reichstein, M., Camps-Valls, G., Stevens, B., Jung, M., Denzler, J., Carvalhais, N., 2019. Deep learning and process understanding for data-driven Earth system science. *Nature* 566 (7743), 195–204.
- Rose, A.W., Hawkes, H.E., Webb, J.S., 1979. *Geochemistry in mineral exploration*. Academic Press, London.
- Salimans, T., Goodfellow, I., Zaremba, W., Cheung, V., Radford, A., Chen, X., 2016. Improved techniques for training GANs. *arXiv:1606.03498*.
- Schlegl, T., Seeböck, P., Waldstein, S.M., Schmidt-Erfurth, U., Langs, G., 2017. Unsupervised anomaly detection with generative adversarial networks to guide marker discover. *Int. Conf. Inform. Process. Med. Imag.* 146–157.
- Shepard, D., 1968. A two-dimensional interpolation function for irregularly-spaced data. *ACM National Conf.* 517–524.
- Sinclair, A.J., 1974. Selection of threshold values in geochemical data using probability graphs. *J. Geochem. Explor.* 3, 129–149.
- Sun, X., Deng, J., Gong, Q., Wang, Q., Yang, L., Zhao, Z., 2009. Kohonen neural network and factor analysis based approach to geochemical data pattern recognition. *J. Geochem. Explor.* 103, 6–16.
- Theis, L., Oord, A. V. D., Bethge, M., 2015. A note on the evaluation of generative models. *arXiv:1511.01844*.
- Vriend, S.P., Van Gaans, P.F.M., Middelburg, J., De Nijs, A., 1988. The application of fuzzy c-means cluster analysis and non-linear mapping to geochemical datasets: examples from Portugal. *Appl. Geochem.* 3, 213–224.
- Wang, C., Rao, J., Chen, J., Ou, Y., Qi, Y., Li, Q., 2017. Prospectivity mapping for “Zhuxi-type” copper-tungsten polymetallic deposits in the jingdezhen region of jiangxi province, south china. *Ore Geol. Rev.* 89, 1–14.
- Wang, D., Shu, L., 2012. Late Mesozoic basin and range tectonics and related magmatism in Southeast China. *Geosci. Front.* 3 (2), 109–124.
- Wang, X., Zhang, Q., Zhou, G., 2007. Nationalscale geochemical mapping projects in China. *Geostand. Geoanal. Res.* 31 (4), 311–320.
- Wang, Q., Zi, F., 2007. Partial melting of thickened or delaminated lower crust in the middle of Eastern China: Implications for Cu-Au Mineralization. *J. Geol.* 115, 149–161.
- Wang, Y., Xue, C., Liu, J., Wang, J., Yang, J., Zhang, F., Zhao, Z., Zhao, Y., Liu, B., 2015. Early Carboniferous adakitic rocks in the area of the Tuwu deposit, eastern Tianshan, NW China: Slab melting and implications for porphyry copper mineralization. *J. Asian Earth Sci.* 103, 332–349.
- Wang, Z., Zuo, R., Dong, Y., 2019. Mapping geochemical anomalies through integrating random forest and metric learning methods. *Nat. Resour. Res.* 28, 1285–1298.
- Wu, X., Gong, Q., Xiang, Y., 2006. Information integration methods on tungsten mineralization from regional geochemical survey data in Nanling district. Discussion

- on the method of extracting tungsten ore information from regional geochemical exploration data in Nanling area. *Computing technology for geophysical and geochemical exploration* 28 (2), 182–187.
- Xie, X., Ren, T., 1993. National geochemical mapping and environmental geochemistry—progress in China. *J. Geochem. Explor.* 49, 15–34.
- Xie, X., Mu, X., Ren, T., 1997. Geochemical mapping in China. *J. Geochem. Explor.* 60, 99–113.
- Xiong, Y., Zuo, R., 2016. Recognition of geochemical anomalies using a deep autoencoder network. *Comput. Geosci.* 86, 75–82.
- Xiong, Y., Zuo, R., 2018. GIS-based rare events logistic regression for mineral prospectivity mapping. *Comput. Geosci.* 111, 18–25.
- Xiong, Y., Zuo, R., 2020. Recognizing multivariate geochemical anomalies for mineral exploration by combining deep learning and one-class support vector machine. *Comput. Geosci.* 140, 104484.
- Xiong, Y., Zuo, R., 2021. Robust feature extraction for geochemical anomaly recognition using a stacked convolutional denoising autoencoder. *Math. Geosci.* <https://doi.org/10.1007/s11004-021-09935-z>.
- Xu, B., Guo, L., Shi, Y., 1992. Proterozoic Terranes and Multiphase Collision Orogens in Anhui-Zhejiang-Jiangxi Area. Geological Publishing House, Beijing (In Chinese with English abstract).
- Yang, M., Huang, S., Lou, F., Tang, W., Mao, S., 2009. Lithospheric structure and largescale metallogenic process in Southeast China continental area. *China Geol.* 36, 528–543 (in Chinese with English abstract).
- Yousefi, M., Carranza, E.J.M., 2015. Prediction-area (P-A) plot and C-A fractal analysis to classify and evaluate evidential maps for mineral prospectivity modeling. *Comput. Geosci.* 79, 69–81.
- Yousefi, M., Carranza, E.J.M., 2016. Data-driven index overlay and boolean logic mineral prospectivity modeling in greenfields exploration. *Nat. Resour. Res.* 25, 3–18.
- Zenati, H., Foo, C. S., Lecouat, B., Manek, G., Chandrasekhar, V. R., 2018a. Efficient GAN-based anomaly detection. arXiv:1802.06222.
- Zenati, H., Romain, M., Foo, C.S., Lecouat, B., Chandrasekhar, V., 2018. Adversarially learned anomaly detection. In: International conference on data mining (ICDM), pp. 727–736.
- Zhao, G., Cawood, P.A., 1999. Tectono-thermal evolution of the Mayuan Assemblage in the Cathaysia Block: Implications for Neoproterozoic collision-related assembly of the South China Craton. *Am. J. Sci.* 299, 309–339.
- Zhao, G., 2015. Jiangnan Orogen in South China: Developing from divergent double subduction. *Gondwana Res.* 27, 1173–1180.
- Zhao, W., Zhou, M., Li, Y., Zhao, Z., Gao, J., 2017. Genetic types, mineralization styles, and geodynamic settings of Mesozoic tungsten deposits in South China. *J. Asian Earth Sci.* 137, 109–140.
- Zhou, J., Wang, X., Qiu, J., 2009. Geochronology of Neoproterozoic mafic rocks and sandstones from northeastern Guizhou, South China: Coeval arc magmatism and sedimentation. *Precambr. Res.* 170, 27–42.
- Zhou, X., Sun, T., Shen, W., Shu, L., Niu, Y., 2006. Petrogenesis of Mesozoic granitoids and volcanic rocks in South China: A response to tectonic evolution. *Episodes* 29 (1), 26–33.
- Zhou, Z., Liu, X., 2006. Training cost-sensitive neural networks with methods addressing the class imbalance problem. *IEEE Trans. Knowl. Data Eng.* 18, 63–77.
- Zuo, R., Cheng, Q., Agterberg, F.P., 2009. Application of a hybrid method combining multilevel fuzzy comprehensive evaluation with asymmetric fuzzy relation analysis to mapping prospectivity. *Ore Geol. Rev.* 35, 101–108.
- Zuo, R., 2018. Selection of an elemental association related to mineralization using spatial analysis. *J. Geochem. Explor.* 184, 150–157.
- Zuo, R., Xiong, Y., Wang, J., Carranza, E.J.M., 2019. Deep learning and its application in geochemical mapping. *Earth-Sci. Rev.* 192, 1–14.